Laser and Particle Beams (1996), *vol.* 14, *no.* 3, *pp.* 293–321
Printed in the United States of America

Corpuscular diagnostics and processing methods applied in investigations of laser-produced plasma as a source of highly ionized ions

By E. WORYNA,* P. PARYS,* J. WOŁOWSKI,* AND W. MRÓZ†
*Institute of Plasma Physics and Laser Microfusion, 23 Hery St., P.O. Box 49, 00-908 Warsaw, Poland
†Institute of Optoelectronics, Military University of Technology, 00-908 Warsaw, Poland

(Received 2 April 1996; accepted 17 April 1996)

This paper presents a set of complementary corpuscular diagnostics applied in experiments for investigation of laser-produced plasma as a source of ions. The measuring possibilities and methods for processing experimental data of a cylindrical electrostatic ion energy analyzer, a Thomson parabola ion analyzer, various types of electrostatic probes, a detector of neutral atom fluxes, as well as methods for visualization of ion emission areas are discussed. Special attention was focused on the ion-induced secondary electron emission problem and its influence on the accuracy of the measurements.

1. Introduction

By corpuscular diagnostics for laser-created plasmas we mean all devices that can give possibilities of measurements of the material particles that are expanded from laser plasmas. The common feature of all corpuscular diagnostics is the fact that they give information about the plasma parameters at long distances from the target, so-called asymptotic parameters of the plasma. In fact, we do not measure the whole plasma but only one component of it, in particular, ions, from which measurements may be deduced using a proper model of plasma expansion and parameters of plasma at the laser focus spot, which means at the place of plasma creation. It is also possible to measure electrons, neutral atoms, and clusters. In spite of this fact, such ion parameters like ion energy distributions, the total number of ions, their average and maximum charge states, the abundance of ion species, and energy carried by them give very precise information about the mechanisms of the laser interaction with plasma, the absorbed energy, the electron temperature of plasma, and others.

Ion diagnostic often is used as a complementary diagnostic, giving additional information to other diagnostic systems (Eidmann *et al.* 1984; Ripin *et al.* 1980; Mróz *et al.* 1989). Ion collector current may be used for monitoring the laser operation, because its magnitude and shape are very sensitive to laser pulse parameters. A set of complementary corpuscular diagnostics can be used as a main diagnostic system for a variety of investigation problems, such as mass ablation rate (Goldsack *et al.* 1982), energy transport (Gusinov *et al.* 1978; Gupta *et al.* 1986), interaction with high-Z targets (Grun *et al.* 1986, Mróz *et al.* 1992a), laser plasma as a source of high ionized ions (Haseroth *et al.* 1994; Láska *et al.* 1994, 1995; Woryna *et al.* 1996), and fast ion investigations (Bocher *et al.* 1978; Decoste *et al.* 1986). It is also very useful in experiments on spherical compression of plasma (Wołowski *et al.* 1985).

In the past years, laser-produced plasma often has been considered and studied as a source of ions from solids (Henkelmann *et al.* 1992; Kutner *et al.* 1992; Amdidouche *et al.* 1992;

© 1996 Cambridge University Press 0263-0346/96 $11.00 + .10

https://doi.org/10.1017/S0263034600010053 Published online by Cambridge University Press

Sharkov *et al.* 1992; Makarov *et al.* 1994; Mróz *et al.* 1994a; Láska *et al.* 1994, 1995; Haseroth *et al.* 1995; Parys *et al.* 1995a,b; Woryna *et al.* 1996). Laser ion sources are especially convenient in the case when a high current of highly charged ions from solids is needed. The most obvious is the use of the laser-ion sources of highly ionized ions for accelerator injection (Barabash *et al.* 1989); various projects of this kind exist, the most prominent among them being the Large Hadron Collider (LHC) project at CERN (Billinge *et al.* 1990; Haseroth & Hora 1993).

In the following paragraphs of this paper, we present selected apparatus for corpuscular diagnostics, which are used or planned to be used in the near future in experiments on investigations of the laser-produced plasma as a source of highly ionized ions.

2. Laser-produced plasma as an object for corpuscular diagnostics

The high-temperature plasma produced as a result of the interaction of high-power laser radiation ($I\lambda^2 \sim 10^{13}$–10^{15} Wcm$^{-2}\mu$m^2) with surfaces of solid-state targets is the only physical object, the lifetime of which is determined by the velocity of plasma expansion as a result of the action of hydrodynamic pressure. The characteristic values of the electron temperature, T_e, and the electron concentration, n_e, are $T_e \sim 100$–1000 eV and $n_e \sim 10^{18}$–10^{23} cm^{-3}. The average velocity of plasma expansion lies in the range $v \sim 10^6$–10^8 cm/s, which corresponds to ion energy of from tens to hundreds of keV, depending on the ion mass. At the front of the plasma expanding into vacuum, in a layer of the thickness comparable to the length of the Debye screening, an essential role is played by ambipolar electric fields that are set up by the hot (fast) electrons leaving the plasma corona. The hot electron population is formed by electron acceleration in the field of electrostatic Langmuir waves, which themselves originate either from the mechanism of resonant absorption of the laser radiation near the critical density surface, or from nonlinear coupling of the primary wave and the ion acoustic wave, or from stimulated Raman scattering of the primary wave on the Langmuir wave (Kruer 1988; Baldis *et al.* 1991).

In this field, an additional kinetic energy is transferred to a small part of the total number of ions. The energy of those accelerated ions, which are referred to as *fast ions*, may be one order of magnitude or more higher than the initial thermal energy of ions. It can vary from hundreds of keV for light ions, like H and C ions (Joshi *et al.* 1979), up to a maximum measured energy of fast Ta ions, about 9 MeV (Láska *et al.* 1995). Velocity distributions of fast ions have an exponential form similar to that for the thermal ions. This and hot electron distributions are the reasons for characterizing the laser-produced plasma by the two-temperature approximation (Wickens & Allen 1981). Charges of ions emitted from laser-produced plasma can vary from one up to at least $z \sim 50$, as was measured for Ta ions (Láska *et al.* 1994; Woryna *et al.* 1995; Láska *et al.* 1994, 1995).

During laser interaction with high-Z targets, a part of the absorbed laser energy is reemitted as X rays from the absorption area. These reemitted X rays escape partially from the plasma, and partially are absorbed again in the solid target outside the laser focus. The absorbed part of radiation creates a solid-state density nonideal (strongly coupled) plasma (Ichimaru 1982) with the temperature $T_e \sim 100$ eV (Eidmann *et al.* 1990; Sigel *et al.* 1990). For Ta and Au targets, the number of ions from X-ray-generated plasma can be about an order of magnitude higher than the number of ions from the thermal plasma (Mróz *et al.* 1992a). These ions have the average energy of a few keV and the average charge state at a long distance from the target $z < 1$. This means that nonionized atoms of target material expand together with ions (Chvojka *et al.* 1994; Mróz *et al.* 1994b). As a result of recombination processes taking place in the plasma during expansion into vacuum, the proportion

https://doi.org/10.1017/S0263034600010053 Published online by Cambridge University Press

of ions of different charges varies. This statement applies in particular to low-energy ions from X-ray–heated plasma and thermal plasma. On the contrary, fast ions expand without practically any changes in their composition (Sadowski *et al.* 1976).

The principle of operation of most of the apparatus described in the following paragraphs is based on the time-of-flight method. This means that the measurement of ion velocity consists in measuring the time of flight, t, of the ions passing the distance L from the plasma focus to the detector. The time-of-flight method is correct in the case when $t \gg \tau$ and $L \gg r$ (where τ is the laser pulse duration and r is the radius of the laser focus spot). As may be seen, corpuscular diagnostics based on the time-of-flight method treat the laser-produced plasma as a point source of ions.

3. Electrostatic cylindrical ion energy analyzer

3.1. *Ion beam shaping and space charge effects in ion energy analyzers*

The emission of ions from laser-produced plasmas expanding into vacuum has been the subject of intensive studies over a number of years. Analyzers often are used to determine the ion energy spectra and the abundance of ion species in the plasma. Because the expanded plasma is, in principle, quasineutral (fast particles can be exceptional), the separation of plasma into ion and electron components must be performed and the electron component should be removed completely. If the separation takes place over the entrance slit of the analyzer placed at a long distance from the ion source, the width of it should be lower than the Debye radius, $b_{in} < \lambda_D$. However, some questions arise about the problem: Does the screening effect of ions really take place? Is the number of charged particles in the Debye sphere sufficiently large, $N_D = (4/3)\pi\lambda_D^3 n_e \gg 1$? In the case of adiabatic expansion of a laser-produced plasma, the electron concentration, n_e, and the electron temperature, T_e, depend on the distance L as follows:

$$n_e = n_{e0}(r_0/L)^m \qquad T_e = T_{e0}(r_0/L)^{m(\gamma-1)}, \tag{1}$$

where n_{e0} and T_{e0} are the initial electron concentration and electron temperature of the plasma, r_0 is the initial radius of the plasma, $m = 1$, 2, or 3, depending on the expansion geometry, and $\gamma (= 5/3)$ is the specific heat ratio. Inserting equations (1) into the N_D formula we find, finally,

$$N_D(L) = N_D(r_0) \cdot (r_0/L)^{m((3\gamma/2)-2)}. \tag{2}$$

For example, considering adiabatic spherical expansion of plasma and taking $T_{e0} = 1$ keV, $n_{e0} = 5 \times 10^{20}$ cm^{-3}, $r_0 = 0.0075$ cm, and $L = 200$ cm, we obtain $\lambda_D(r_0) = 1.1 \times 10^{-6}$ cm, $\lambda_D(L) \approx 1.7 \times 10^{-4}$ cm, $N_D(r_0) \approx 2.8 \times 10^3$ electrons, and $N_D(L) \approx 6.4 \times 10^{-4}$ electrons. It is seen that, for a large distance from the target, the screening effect of ions is not valid. From the above considerations we have the result that, in the case of adiabatic spherical expansion, the condition for plasma separation in ion analyzers will be in the following form:

$$U/\Delta R \gg 4\pi z e n_i b_{in}, \tag{3}$$

where U and ΔR are the voltage and the spacing between the plate of the analyzing system, respectively, n_i is the ion concentration with the charge state z, b_{in} is the width of the entrance slit, and e is the elementary charge. Equation (3) shows that the electric field in the ion analyzer should be much higher than the electric field due to the charge separation of a plasma.

https://doi.org/10.1017/S0263034600010053 Published online by Cambridge University Press

The adiabatic expansion can be disturbed due to the recombination heating of a plasma. However, in the case of spherical expansion, and with the electron temperature changing as $T_e \sim 1/L$, the number of particles in the Debye sphere is constant. That is the case in which the electron temperature is needed to estimate the $\lambda_D(L)$.

Ion current densities in the range of several mA/cm^2 may be expected from laser-produced plasma at long distances from the target. This suggests that a sufficient influence of charge space effects will occur. The influence of charge space effects on the energy resolution of ion particle analyzers has been discussed by a number of workers (Fleischmann *et al.* 1965; Green 1970). Green (1970) gave the condition limiting the usable plasma density $n_i(L)$ [cm^{-3}] for which space charge effects could be neglected,

$$n_i \leq 5 \times 10^8 \frac{E}{l^2 z} \frac{b_{out}}{b_{in}}, \tag{4}$$

for strip ion beams, where b_{out}/b_{in} is the ratio of the entrance-to-output width, E [keV] is the energy of ions with the charge state z, and l [cm] is the path of flight of ions inside the analyzing system.

3.2. *Principle of operation*

The mass spectrometer described below is an electrostatic cylindrical ion energy analyzer (IEA) combined with the time-of-flight method designed for the diagnostics of pulsed ion sources. In particular, it is used for measurements of laser-produced plasmas. The main part of the IEA is the deflection system. It is a sector of two coaxial metallic cylinders of radii R_1 (inner plate) and R_2 (outer plate) maintained at potentials V_1 and V_2, respectively, and with deflection angle ψ (figure 1). The radial electric field inside the deflection system is given by

$$E_r = (V_2 - V_1)/[r \ln(R_2/R_1)], \tag{5}$$

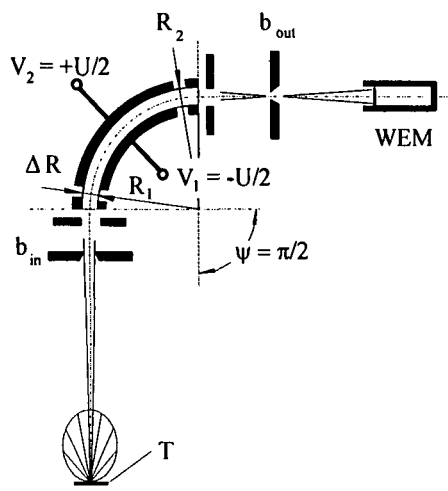

FIGURE 1. Schematic drawing of the IEA. R_1, R_2, R_0, ΔR—inner, outer, and mean radius of the deflection plates, and the gap between them, respectively; $|V_2| = V_1 = U/2$—potential of the deflection plates; b_{in}, b_{out}—width of the input and output slits, respectively; Ψ—deflection angle of the deflection plates; WEM—detector (windowless electron multiplier); T—target.

https://doi.org/10.1017/S0263034600010053 Published online by Cambridge University Press

where r is the radius of an equipotential surface and $R_1 \leq r \leq R_2$. In most cases of symmetric polarization, $V_2 = -V_1 = U/2$, the equipotential surface $V_0 = 0$ exists for

$$r = R_0 = (R_1 R_2)^{1/2} \cong (R_1 + R_2)/2, \tag{6}$$

at $R_2 - R_1 = \Delta R < R_0$, when R_0 is the mean radius of the deflection plates. If a particle with the charge ez, mass M, and velocity v is to have a circular trajectory with $r = R_0$, the following force equation must be held:

$$Mv^2/R_0 = ezE_r(R_0), \tag{7}$$

or, equivalently,

$$E/z = eR_0 E_r(R_0) = eU/[2\ln(R_2/R_1)] \cong \kappa eU, \tag{8}$$

where $\kappa = R_0/(2\Delta R)$ is the geometric factor of the IEA and E is the kinetic energy of the particle. From equation (8), we have that only ions with a given energy-to-charge state ratio, E/z, can pass through the IEA, that is, the IEA is operated as an energy filter.

Ions are separated on the path of flight L from the ion source to the detector due to their energy spread. The time of flight of ions from the ion source to the detector is

$$t = L(M/2E)^{1/2} = L[M/(2ez\kappa U)]^{1/2}. \tag{9}$$

It can be seen from equations (8) and (9) that only ions with particular values of their mass-to-charge state ratio, M/z, can pass through the IEA and reach the detector.

More detailed information on the electrostatic analyzers for charged particle beam measurements can be found in the monographs by Kozlov (1971) and Afanas'ev and Yavor (1978).

3.3. *Analyzer design*

A schematic drawing of the IEA is shown in figure 1. Our IEA was constructed to be used in laser–plasma interaction experiments for a variety of target materials and laser–plasma interaction experiments. The first version of the IEA (Denus *et al.* 1977) had a controlled width of input and output slits. In addition, the output slit had the possibility to be moved in the axial direction to optimize the width and the distance from the edge of the deflection system (electrostatic field). As a detector, a windowless electron multiplier (WEM) was used. The construction enabled us to measure the transmission coefficient of the IEA, k' (i.e., the ratio of the number of ions at the output slit and the number of ions after the input slit), and the gain, $K = k'G$, of the IEA–WEM set, where G is the gain of the WEM. The calibration experiment (Denus *et al.* 1977), performed with a continuous H^+ ion beam of energy up to 3 keV, revealed that the gain of that set was independent of the ion energy at a fixed width of the input and output slits. Our experience and experimental results obtained have enabled us to construct a new IEA with a simpler construction and better operational parameters. The main parameters are listed in table 1.

3.4. *Resolution*

One of the basic characteristics of a mass spectrometer is its resolving power. The mass resolution of an electrostatic analyzer is given by

$$R_m = m/\Delta m = t/(2\Delta t), \tag{10}$$

where $m = (m_1 + m_2)/2$, $\Delta m = m_1 - m_2$, $m \equiv m_k (k = 1, 2)$ denotes the mass-to-charge state ratio, $m_k = M_k/z_k$, t is the time of flight of an ion that may be resolved from a neighboring ion, and Δt is the time distance between the resolved ion pulses (figure 2). The width

https://doi.org/10.1017/S0263034600010053 Published online by Cambridge University Press

TABLE 1. The main parameters of the IEAs

Parameter	Value	
	First Version	Second Version
Deflection angle, Ψ, rad	$\pi/2$	$\pi/2$
Radius of the outer deflection plate, R_2, cm	10.5	9.5
Radius of the inner deflection plate, R_1, cm	10.25	9.75
Mean radius of the deflection system, R_0, cm	10	10
Gap between the deflection plates, ΔR, cm	1.0	0.5
Height of deflection plates to gap width ratio	3.5	7.0
Geometric factor of the IEA, $\kappa = R_0/(2\Delta R)$	5	10
Maximum potential of deflection plates, $U/2$, kV	4.0–6.0	12.0
Maximum energy-charge state ratio, E/z, keV	40–60	240
Energetic dynamic range, $D = E_{max}/E_{min}$	2.0×10^4	4.5×10^4
Input slit:		
accuracy of control, Δb_{in}, μm	± 10	± 10
width range, b_{in}, mm	0–5	0–5
Output slit:		
accuracy of control, Δb_{out}, μm	± 10	none
width, b_{out}, mm	0–5	1
Detector	windowless electron multiplier (WEM)	
Pressure, Torr	4×10^{-6}	
Weight, kG	about 6	

of an ion pulse entering the detector may be described as follows (Bykovskii & Nevolin 1985):

$$\Delta\tau = \Delta\tau_1 + \Delta\tau_2 + \Delta\tau_3 + \Delta\tau_4, \tag{11}$$

where $\Delta\tau_1$ is the broadening of the ion pulse caused by ion emission duration, $\Delta\tau_2$ is the broadening caused by the finite width of the output slit of the IEA, $\Delta\tau_3$ is the broadening due to divergence of the ion beam in the input slit of the IEA, and $\Delta\tau_4$ is the broadening due to the space-charge effect behind the input slit of the IEA. The $\Delta\tau$ width was

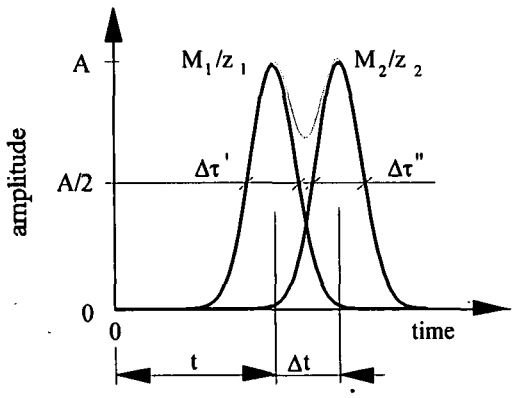

FIGURE 2. Explanation of notations used for resolving power determination. t—time of flight; Δt—time interval between resolved ion pulses; M_1/z_1, M_2/z_2—mass to charge state ratio of resolved ion pulses; $\Delta\tau'$,$\Delta\tau''$—FWHM of ion pulses entering the detector; A—amplitude of ion pulses.

https://doi.org/10.1017/S0263034600010053 Published online by Cambridge University Press

estimated by taking into consideration the parameters of our IEA and the measuring geometry used in the experiments presented in Haseroth *et al.* (1995), and we obtained the mass resolving power $R_m = t/(2\Delta t) \approx 150$.

Experimentally, the power resolution of the IEA was determined in Mróz *et al.* (1992b) for $^{104}Pd^+$ and $^{105}Pd^+$ isotopes, and it was $R_m \geq 105$. From the experimental data (Haseroth *et al.* 1995), we can conclude that $47 < R_m < 180$ [the limits correspond to fully resolved ion pulses of tantalum ions and unresolved ion pulses of C^{3+}, O^{4+}, and Ta^{45+} (figure 3)]. The maximum value of the R_m determined experimentally is consistent with the theoretical one.

3.5. *Methods for processing the experimental results*

In our experiments, the recording process of ion spectra is fully automated. The ion oscillograms were registered using multichannel digitizing oscilloscopes (Tektronix TDS 460, TDS 540, DSA 601A, and Hewlett-Packard HP 54540). As an example, figure 3 (Láska

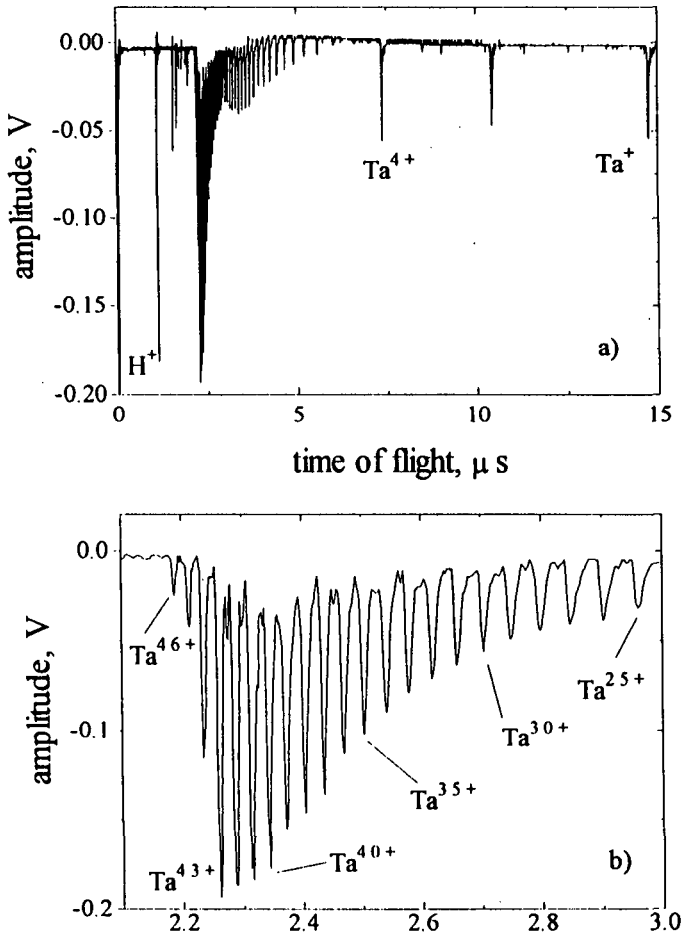

FIGURE 3. Ion spectrum of Ta ions in two different time scales (Láska *et al.* 1995). Experimental: iodine laser *PERUN*: energy 20.2 J in 300 ps, $\lambda = 0.438$ μm (third harmonic), $L_{IEA} = 211$ cm, $E/z = 400$ keV.

https://doi.org/10.1017/S0263034600010053 Published online by Cambridge University Press

et al. 1995) shows recorded Ta ion spectrum from the IEA. Then, the recorded oscillograms were computer-processed to obtain information about the plasma under investigation. The results of processing are shown in Woryna *et al.* (1994) and Láska *et al.* (1995). It is possible to identify clearly all ion species occurring in the recorded ion spectra using equations (8) and (9), with the exception of those having the same or nearly the same M/z ratio for a given E/z.

The relation combining the measured voltage amplitude, $U_z(t)$ for a given z, and the number of ions reaching the WEM, dN_z/dt (into the solid angle of the input slit), is

$$dN_z/dt = U_z(t)/(e\gamma_z R_{load} K), \tag{12}$$

where e is the electron charge, γ_z is the secondary ion-electron emission coefficient, $K = k'G$ is the gain of the IEA–WEM set, k' is the transmission coefficient of the IEA, G is the gain of the WEM, R_{load} is the load resistance, and t is the time of flight of the considered ion.

Generally, γ_z for a given target (dynode material of the WEM) depends on the atomic mass, charge state, and energy of ions impacting on the target. The effect of secondary ion-electron emission will be discussed in Section 8.

Using very simple transformation formulas, $dN/dv = (dN/dt)(dt/dv)$ and $dN/dE = (dN/dv)(dv/dE)$, we can obtain relations that make it possible to calculate the amplitudes of velocity and energy distributions, dN_z/dv and dN_z/dE, respectively:

$$dN_z/dv = (dN_z/dt)L/v^2 = LU_z(t)/(eR_{load}v^2\gamma_z K), \qquad v = L/t, \tag{13}$$

$$dN_z/dE = (dN_z/dv)/(mv) = LM^{1/2}U(t)/[eR_{load}\gamma_z K(2E)^{3/2}], \qquad E = ML^2/(2t^2), \tag{14}$$

where v is the ion velocity. Equations (12), (13), and (14) make it possible to determine any of the distributions mentioned above.

In order to get the time, velocity, or energy distributions of ions, a large number of ion spectra have to be measured at settled working conditions of the laser system (energy and duration of laser pulses) and with changing the deflection potential, $\pm U/2$, from one laser shot to another. In our experiments, ion collector oscillogram shapes served as an indicator of the laser operation, and only those ion spectra were used to process the data from the IEA.

The number of particular ion species may be determined by integrating any of the distributions, for example, the energy distributions of ion species:

$$N_z = \int_{E_{\min}}^{E_{\max}} (dN_z/dE)dE, \tag{15}$$

because the total number of ions is

$$N_T = \sum_{i=1}^{z_{\max}} N_i. \tag{16}$$

The average charge state of the plasma can be determined from:

$$\bar{z} = \sum_{i=1}^{z_{\max}} iN_i/N_T. \tag{17}$$

The abundance of ion species is

$$a_z = N_z/N_T. \tag{18}$$

https://doi.org/10.1017/S0263034600010053 Published online by Cambridge University Press

The main disadvantage of the IEA is the requirement of a large number of laser shots under repetitive working of the laser system to obtain the results searched. Now, to our knowledge, only two types of analyzers exist, by means of which it is possible to record, in one laser shot, many time distributions of ion species, $dN_z(t)/dt$. These are the Thomson parabola ion analyzer described in Section 4, and the analyzer with pulsed voltage deflection system (Chowdhury *et al.* 1980). But both analyzers have a much lower dynamic range and resolution.

4. Thomson parabola ion analyzer

4.1. *Principle of operation*

The mass spectrograph of the Thomson type (TP) presented here (figure 4) is a new version of the TP used earlier (Farny *et al.* 1979) in the experiments on plasma compression in the KALMAR laser system, which was based on a scheme described by Olsen *et al.* (1973). Our construction is based on the configuration described by Slater (1978). In the Thomson parabola analyzer (Thomson 1911), charged particles are deflected by static electric and magnetic fields parallel to each other and perpendicular to the charge particle stream. The principal assemblies of the TP are the system of two diaphragms, the first of which also plays the role of ion collector, and the deflection chamber with the electric and magnetic fields and registration system.

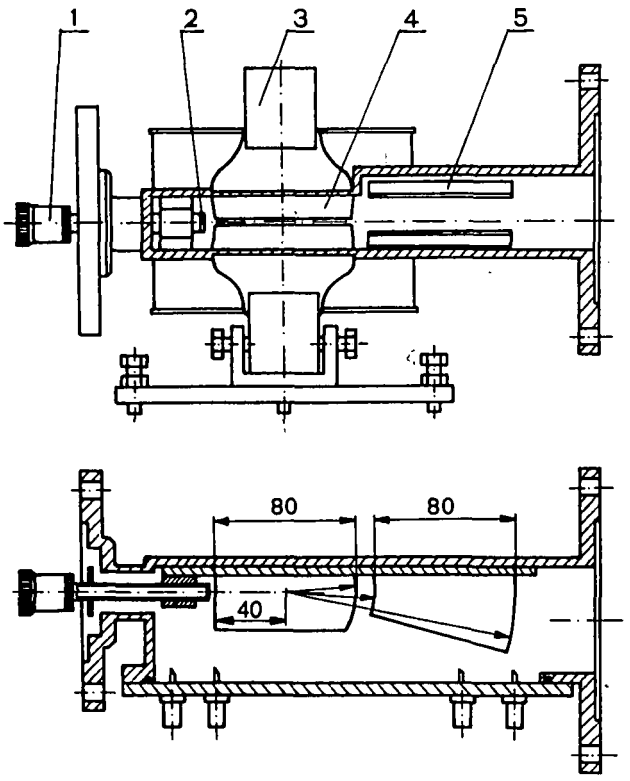

FIGURE 4. The top and side views of the deflection chamber of the TP. 1—the first diaphragm and the ion collector, 2—the second forming diaphragm, 3—electromagnet, 4—pole shoes of electromagnet, 5—deflecting condenser plates (R_1 = 40 mm, R_2 = 50 mm, R_3 = 130 mm).

https://doi.org/10.1017/S0263034600010053 Published online by Cambridge University Press

Shaping of an ion beam is made by the system of two diaphragms. The first one, the diameter of which can be changed from 0.5 to 2 mm, is used together with the second diaphragm for alignment of the main axis of the TP, which is defined by the laser focus on the target and by neutral point on image converter. The first diaphragm is made as a hole in the plate used as an ion collector, and may be negatively polarized. Sometimes it can be used for reduction of the plasma concentration. By changing the diameter of it, we can influence the plasma concentration in the plane of the second forming diaphragm. The forming diaphragm of diameter 100 μm is used for the final formation of the ion beam before deflecting plates. It is about 2 mm away from the electromagnet shoes. The drift tube between the first and second diaphragms was made from soft iron to screen drifting ions from the magnetic field. When the TP operates far from the laser target (0.5–1 m), it is enough to use only one diaphragm, the second.

Ion separation is made in the deflection chamber, which is the stainless steel vacuum chamber containing the pole shoes of an electromagnet, made from soft iron, and deflecting condenser plates. The electromagnet used in the analyzer was designed to provide accurate velocity measurements over wide energy and M/z ratio ranges of the registered ions. The maximum possible magnetic field in the deflection chamber is about 8 kGs, which is much more than is needed for the measurements of even very energetic ions. For the measurements of highly charged tantalum ions with energies of a few MeV (figure 5), it was enough to use a magnetic field of $B \sim 500$ Gs. The magnetic field, B(Gs), in the area of ion deflection, can be expressed by the relation (for $0 < I < 2000$ mA):

$$B[\mathrm{Gs}] = 15.38 + 1.03 \times I[\mathrm{mA}], \tag{19}$$

where I(mA) is the electromagnet current.

Separation of the electric and magnetic fields gives the possibility of maximizing the length (80 mm) to the gap (5 mm) ratio in the magnet and minimizing the influence of stray and fringing fields on the measurements. Independently, the magnet-pole edge profiles were profiled especially to minimize the fringing fields, so the effective field boundary was very nearly the same as the physical pole edge (Braams 1964). Two deflecting condenser plates were located 10 mm after the magnet poles. Each was a length of 80 mm, and the distance between them was equal to 21.5 mm. The pole shoes of the electromagnet and deflecting condenser plates were especially profiled to secure all ions to have the same pathway in the deflecting fields.

The diaphragms, the deflection chamber, and the registration system were mounted on a table, which was capable of being moved in three linear directions and provided chamber rotation in relation to the target system by a spherical bearing joint. This junction is very useful in the cases when all TP systems have to be aligned after changing the detector, or when they need detailed correction in vacuum.

From the solution of the motion equation of a charged particle entering at the normal direction into the region of parallel fields, **E** and **B**, we can obtain, assuming a small deflection of ions, the coordinates of the points in which the ions of relevant parameters will be located in the recording plane:

$$x = \alpha zeU/E, \tag{20}$$

$$y = \beta ezB/(ME)^{1/2}. \tag{21}$$

After eliminating E, we have:

$$x = (\alpha MU/\beta^2 ezB^2)y^2, \tag{22}$$

where $\alpha = D_1 l/(2d)$, $\beta = D_2 l/\sqrt{2}$, U is the potential difference between the electrostatic deflecting plates, z and M are the ion charge and mass, respectively, $D_i - l/2$ is the dis-

https://doi.org/10.1017/S0263034600010053 Published online by Cambridge University Press

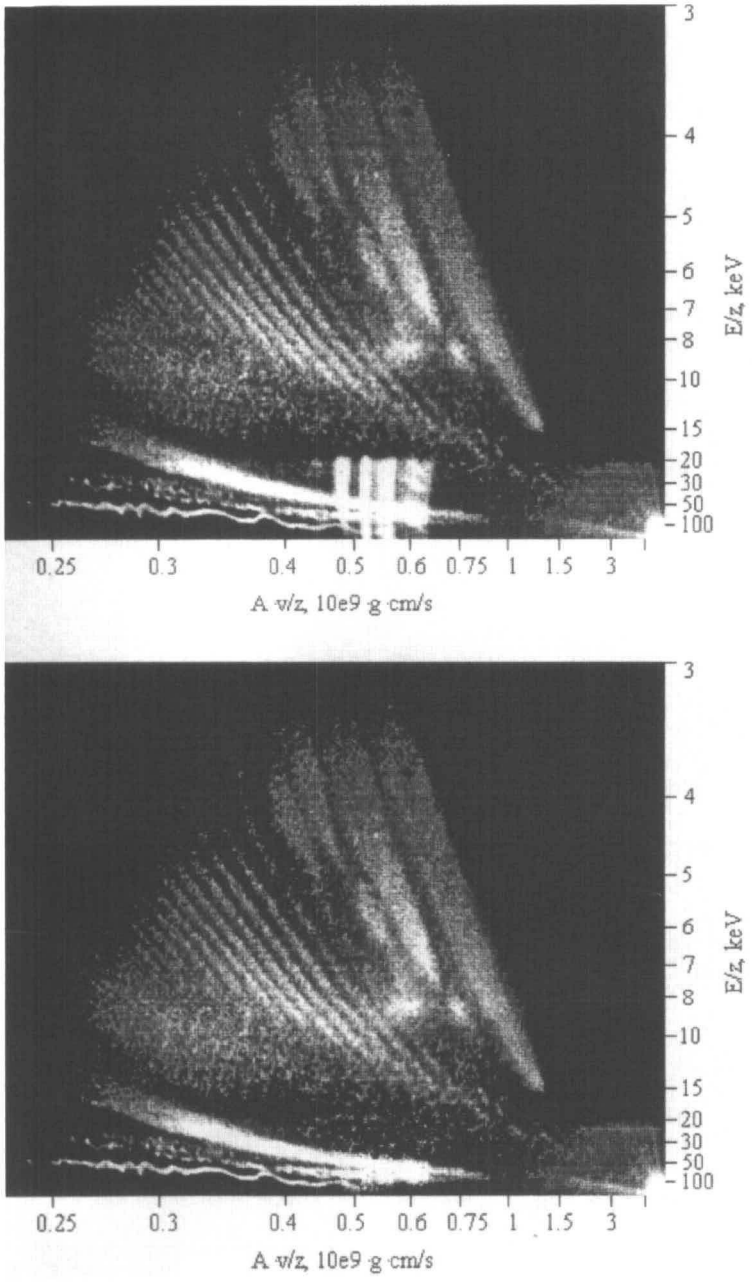

FIGURE 5. Parabolas from Ta targets registered by the Tektronix Video Camera C1002: (a) partially overexposed, (b) the same parabolas after numerical subtraction of overexposure.

tance from the ends of the deflecting plates to the registration plane, and l is the length of the deflecting plates ($l_1 = l_2 = l = 80$ mm, $D_1 = 385$ mm, and $D_2 = 475$ mm).

Equation (18), which describes a parabola, is known as the equation of Thomson parabolas. From this equation, it is inferred that the ions of identical M/z ratios are arranged in the same parabola for fixed values of U and E, the ions of higher energy being located

https://doi.org/10.1017/S0263034600010053 Published online by Cambridge University Press

near the apex of the parabola. It should be observed that a fixed x corresponds to a fixed ratio E/z = const on all parabolas:

$$E/z = \alpha eU/x. \tag{23}$$

Now, the points of intersection of parabolas with the line x/y = const, that is, the line passing the origin of the coordinates, Oxy, correspond to ions of fixed velocity, v, equal to:

$$v = \sqrt{2}(\alpha/\beta)(U/B)(y/x); \tag{24}$$

they are independent of M and z, and any of their combinations M/z. Points of different parabolas lying on the vertical line (y = const) have the same ratios Mv/z:

$$Mv/z = \sqrt{2}\beta eB/y. \tag{25}$$

The recording system of the TP has an adaptability to two different types of detectors: track detectors and an image converter with an MCP of high diameter as an amplifier. Track detectors are the most often used detectors for particle registration in the Thomson spectrographs (Ehler *et al.* 1980; Herold *et al.* 1981; Slater 1978). They could give the number of ions, but they have two inconveniences: the threshold sensitivity for ion registration of about 10–20 keV/amu, which moves the energetic threshold for heavy ion detection to hundreds of keV, and time-consuming treatment of ion tracks, which limits their application in experiments.

The use of microchannel plates (MCPs) as detectors in the TP seems to be very encouraging, especially for low-Z targets (Farny *et al.* 1979; Wołowski *et al.* 1985; Weber *et al.* 1986; Kieffer *et al.* 1985). The application of high-diameter (~90 mm) MCPs has given new possibilities for the TP, such as its use for high-Z ion registration (for Au targets: Mróz *et al.* 1992a, for Ta targets: Woryna *et al.* 1994).

The image converter that we used was composed of an amplifier with an MCP (a rectangle of the size of about 60 × 90 mm of Russian production) with a luminescence screen deposited on a fiber optics. Such construction made it possible to use contact, lensless photography to eliminate light losses, thus improving the recording sensitivity of all converters. In the past few years, we have started to use a Tektronix Video Camera C1002 with a high-sensitivity CCD array as a detector. This camera gives digital pictures of recorded parabolas, which permits automation of all of the measuring processes. Digital processing gives wide possibilities of presentation and correction of registered parabolas, such as contrasting, picturing from given level of exposition, and so on. In figure 5a, we present a picture of parabolas partially overexposed by laser light reflected from different diagnostic systems in the direction of the CCD camera. In figure 5b, the same parabolas can be seen after subtraction of this overexposure.

4.2. *Resolution of the TP*

The problem of the mass and energy resolution for the TP is much more complicated than for the IEA. Generally, each point on an ion energy distribution processed from the same laser shot is counted from experimental data measured with different energy and mass resolutions. To see this, we start from the energy resolution of the TP. By differentiating the formula (16) for ion deflection in an electrostatic field, we can show the influence of all parameters on energy error:

$$dE/E = |d\alpha/\alpha| + |dU/U| + |dx/x|. \tag{26}$$

The first two components are not changeable during the measurements made for the same laser shot, and their sum is of the order of the second component. $\Delta U/U \sim$ 2–3% (for estimation of the energy error, we have passed from differential to real errors; for exam-

https://doi.org/10.1017/S0263034600010053 Published online by Cambridge University Press

ple, $dU/U \cong \Delta U/U$). In the MCP that we used, deflection x may be changed from 0 to 60 mm. The widths of parabolas are not a persistent parameter. They can vary from hundreds of micrometers up to a few millimeters (see figure 5). The parabola width is influenced mainly by the quantity and charge state of the ions, the time of flight (ion energy) from the forming diaphragm to the MCP, and the geometry of the measurements, especially when only one diaphragm (working as a pinhole camera) is used. As an example, we take ions with $E/z = 10$ keV, that is, ions laying on the fragments of different parabolas with the same deflection x. The energy of ions with $z = 1$ is $E(z = 1) = 10$ keV, and the energy of ions with $z = 10$ is $E(z = 10) = 100$ keV. If we take the time of flight of ions with $z = 1$ as $t(z = 1) = 1$, then for $z = 10$ it will be $t(z = 10) = 0.32$. As can be seen, the time of flight of ions from the forming diaphragm to the MCP is $t \sim 1/E^{1/2}$. In this time the ion beam expands perpendicularly to its axis as a result of the effect of thermal spreading of ions and the space-charge effect. With the assumption of movement with acceleration, the electrostatic extension of the ion beam will be $dx \cong \Delta x = \Delta R \sim t^2 \sim 1/E$. The part of the parabola of ions with $z = 1$ and $E = 10$ keV will be ten times wider than the part of the parabola of ions with $z = 10$ and $E = 100$ keV. This effect will be enlarged if the number of lowly charged ions is much higher than the number of highly charged ions, and probably may be enlarged as a result of the electrostatic extension of electron beams between the MCP and the luminescence screen. Such a case is very common for laser-produced plasma and is seen in figure 5. The component $\Delta x/x$ can vary for the experimental results from one laser shot to another within 1–50, and it is decisive to the energy resolution of the TP.

Similar analyses may be done to estimate the mass resolution, $R_m = m/\Delta m$, of the TP. The maximum possible error of the mass estimation can be expressed by the formula:

$$dm/m = 2|d\beta/\beta| + 2|dB/B| + |dE/E| + 2|dy/y|. \tag{27}$$

The first two components are not changeable during measurements made for the same laser shot, and their sum is of the order of the second component, $\Delta B/B \sim 2$–3%. The deflection error, $\Delta y/y$, is, similarly to $\Delta x/x$, changeable with position on the parabola. The deflection y for our MCP may be changed from 0 to 80 mm.

The maximum experimentally achieved resolution can be estimated from measurements made with tantalum targets (Woryna *et al.* 1994). The charge state of Ta ions up to $z = 17$ was resolved (the highest charge states not in the full energy ranges). From equation (6) we get the mass resolution $R_m \leq 34$. Those measurements were not optimized to obtain the maximum mass or energy resolution. Instead, we were interested in estimating the maximum energy ranges of ion species.

4.3. *Methods for processing the experimental results*

Irrespective of the detector used, processing the experimental results is very similar to that described for the EIA, and it leads to the preparation of ion energy distributions for each ionization state of registered ions, dN_z/dE. For the present measurements, it was impossible to calibrate the whole recording system, the image converter, and the detector (CCD camera or photographic film), because of the lack of data relating to the variation of the secondary ion-electron emission coefficients, $\gamma_z \equiv \gamma(z,E,M)$, with charge state, energy, and mass. More consideration of this problem is presented in Section 8.

In our experimental practice, we assumed that the registered number of ions, having charge state z and energy E, was proportional to the luminescence intensity, $I(z,E)$, of the TP screen: $N(z,E) = f[I(z,E)] = \text{const} \times I(z,E)$. With this assumption we have:

$$dN(z,E)/dE \sim I(z,E) \times \Delta E, \tag{28}$$

https://doi.org/10.1017/S0263034600010053 Published online by Cambridge University Press

where ΔE is the energetic spreading of ions determined by the element reading the value $I(z,E)$ (the photometer slit or the size of CCD array pixel).

From the function $dN(z,E)/dE$, one can estimate, like for the IEA, the number of particular ion species, N_z, the total number of ions, N_T, the average charge state of plasma, $\bar{z}$, and the abundance of ion species, a_z.

The influence of charge-space effects (radial expansion of the ion beam) on the energy resolution obtainable with deflection-type analyzers is an important question in ion measurements. As a result of charge-space effects, the resolution can decrease, and the proportionality between the input and output signals can disappear. The problems were considered by Fleischmann *et al.* (1965) and Green (1970). Fleischmann *et al.* (1965) discussed errors that may arise in deflection-type analyzers due to radial expansion of an ion beam. The considered effect is clearly seen on the Thomson parabola image shown in figure 5. It can be seen that ions with lower energy (see for example the parabolas corresponding with $z = 1$–4) but lying on the same parabola are more affected by the space charge than ions with higher energy, that is, the parabola is wider in the range corresponding with the ions with lower energy. Taking into account ions with a given E/z, it can be seen that ions with lower z but higher concentration are more influenced by the space-charge effects than ions with higher z and higher energy.

5. Electrostatic probes

Laser-produced plasma experiments frequently use electrostatic probes, that is, charge collectors (Farny 1985; Kozochkin *et al.* 1993; Mróz *et al.* 1994b; Haseroth *et al.* 1995) and Langmuir probes (Koopman 1971; Chang *et al.* 1977; Denus *et al.* 1977; Segall & Koopman 1973). They are the simplest measurement arrangements used to monitor the plasma expansion characteristics and to obtain information about plasma, both in the hot area of plasma and at long distances from the target. However, the quantitative results obtained with their use often are questioned due to the influence of the secondary ion-electron emission coefficient. They include the whole group of probes with one to a few electrodes.

5.1. *Plane electrostatic probes and Faraday cups*

5.1.1. *Principle of operation*

The most common type of probes are plane collectors or Faraday cups (with one or two grids) for ion and electron component separation. The separation usually is done by means of a static electric field that exists between either the grounded entrance grid and the biased (negative) collector (Goforth 1976, Woryna *et al.* 1994; Haseroth *et al.* 1995) (figure 4a) or the grounded entrance grid and the biased (negative) control grid (Pelah 1976; Pearlman 1977) (figure 4b). The ion current is collected by a collector; but once it is reached, it causes a secondary ion-electron emission that affects the ion current measurement. The effect of the secondary emission may be either suppressed or allowed for using Faraday cups, especially a honeycomb-type (Pelah 1976; Pearlman 1977; Raven *et al.* 1980) and a magnetic filter (Pelah 1976).

The theory of the electrostatic probes in the flowing plasma can be found in Kozlov (1969). It results from the theory that the ion current density, i_i, of ions reaching the collector in the absence of the secondary ion-electron emission and shielding grids is (Kozlov 1969)

$$i_i = en_e v = ev \sum_{j=0}^{z_{\max}} z_j n_{i,j}, \tag{29}$$

https://doi.org/10.1017/S0263034600010053 Published online by Cambridge University Press

where n_e is the electron density, j is the number of ion species, $n_{i,j}$ is the density of the jth ion specie, v is the plasma velocity, and z_j is the charge state of the jth ion specie.

In the case of a biased collector, the collector is shielded from the plasma by a space-charge layer (Kozlov 1969). The latter can modify the collector current or alter the secondary ion-electron emission current. The threshold ion density for this effect (Green 1970) is given approximately by

$$n_{i,z} \leq 2.5 \times 10^8 E/(zl)^2, \tag{30}$$

where E(keV) is the kinetic energy of ions with the charge state z, l(cm) is the grid-collector spacing, and $n_{i,z}$(cm^{-3}) is the density of ions with the charge state z. It can be seen from equation (30) that ions with lower energy and charge state are more severely limited by the space charge, which was observed experimentally (Pearlman 1977).

5.1.2. *Processing method for charge collector signals*

In the case of the charge collector type shown in figure 6a, the output current in the collector circuit, I_c, is a combination of ion current, I_i, and secondary electron current, I_e:

$$I_c = I_i + I_e = e\epsilon v S \left\{ \sum_{j=0}^{z_{\max}} [z_j(t) + \gamma_z(t)] n_{i,j}(t) \right\}, \tag{31}$$

where ϵ is the transparency of the entrance grid, $S = \pi d^2/4$ is the area of the collector, d is the diameter of the entrance aperture of the collector, γ_j, z_j, and $n_{i,j}$ are the secondary ion-electron emission coefficient, the charge state, and the density of the jth ion species

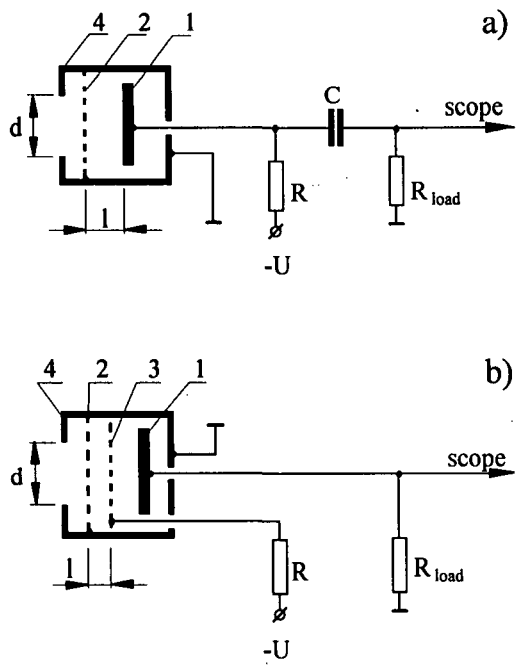

FIGURE 6. Schematic drawing of typical charge collectors used in laser-produced plasma investigations. 1—collector, 2—entrance grid, 3—control grid, 4—grounded housing, R_{load}—load resistance, U—bias potential, l—spacing for electron and ion components separation.

https://doi.org/10.1017/S0263034600010053 Published online by Cambridge University Press

($j = 0$ corresponds to neutral particles), respectively. Taking into account that $n_i = \Sigma n_{i,j}$, we obtain from equation (31)

$$I_c(t) = \epsilon e v S \bar{z}(t) n_i(t) [1 + \bar{\gamma}(t)/\bar{z}(t)] = \epsilon [1 + \bar{\gamma}(t)/\bar{z}(t)] I_{coll}(t), \tag{32}$$

where $\bar{\gamma} = \sum_j \gamma_j n_{i,j} / \sum_j n_{i,j}$ and $\bar{z} = \sum_j z_j n_{i,j} / \sum_j n_{i,j}$ are the average secondary ion-electron emission coefficient and the average charge state of ions, respectively, and I_{coll} is the ion current in the entrance grid for a given moment t. Thus,

$$I_{coll}(t) = U_c(t)/\{\epsilon R_{load}[1 + \bar{\gamma}(t)/\bar{z}(t)]\} = ed[N(t)\bar{z}(t)]/dt, \tag{33}$$

where $U_c(t)$ is the voltage amplitude of the collector signal, $N(t)$ is the number of ions reaching the charge collector, and R_{load} is the load resistance. Thus, the time distribution of ion charge, Q, is

$$dQ/dt = ed[N(t)\bar{z}(t)]/dt = U_c(t)/\{\epsilon R_{load}[1 + \bar{\gamma}(t)/\overline{z(t)}]\}. \tag{34}$$

From equation (34) we can obtain, in a similar way as for the IEA, the velocity, dQ/dv, and energy, dQ/dE, distributions of ion charge; and by integrating them it is possible to obtain the total charge and the total energy carried by ions, as well as the mean energy of ions defined as follows:

$$\langle E \rangle = M(L/\bar{t})^2/2, \tag{35}$$

where

$$\bar{t} = \int_0^\infty f(x)x dx \Big/ \int_0^\infty f(x) dx, \qquad f(t) = U_c(t)/[1 + \bar{\gamma}(t)/\bar{z}(t)].$$

The apparatus described in Sections 3 and 5.1 makes it possible to determine the electron temperature, T_e, and the average charge state, $\bar{z}_0$, of plasma in the region of interaction of laser radiation with plasma. From the relation of asymptotic mean energy of ions [equation (35)] with T_e and $\bar{z}_0$, $\langle E \rangle = C(\bar{z}_0 + \alpha)T_e$, assuming an adequate model of plasma expansion and the $\bar{z}_0 = \bar{z}_0(T_e)$ relation (for example, Shearer & Barnes 1972; Busquet 1982; Farny & Woryna 1987), one can estimate T_e and $\bar{z}_0$. The C factor ($C = 3.33$–5) depends on the accepted model of plasma expansion and the temperature ratio $\alpha = T_i/T_e$, where T_i is the ion temperature of the plasma.

As an example, figure 7 shows the ion collector signal recorded by means of the charge collector-type shown in figure 6a.

In order to obtain information on the space properties of expanding plasma, that is, on angular distributions of plasma parameters, a few charge collectors must be used in experiments, located at various angles Θ with respect to the normal to the surface of the target (or incident laser beam). In Lewis *et al.* (1982), the angular distribution of plasma parameters, $P(\Theta)$, were approximated by the $P(\Theta) = P \cos^n \Theta$ function. The angular distributions can be approximated by a more universal formula in the following form: $P(\Theta) = P(\Theta_1) \cos^m \Theta + P(\Theta_2) \sin^n \Theta$. Integration of these gives the total value of the determined parameter of plasma,

$$P_{total} = 2\pi \int_0^{\pi/2} P(\Theta) \sin \Theta \, d\Theta, \tag{36}$$

where $P(\Theta_1)$ and $P(\Theta_2)$ are the magnitudes of the P parameter at angles Θ_1 and Θ_2, respectively.

The ratio $\bar{\gamma}/\bar{z}$ will be discussed in Section 8.

All of the above-mentioned relations are valid for Faraday cups or secondary emissionless charge collectors (Raven *et al.* 1980; Eidmann *et al.* 1984; Kozochkin *et al.* 1993) if

https://doi.org/10.1017/S0263034600010053 Published online by Cambridge University Press

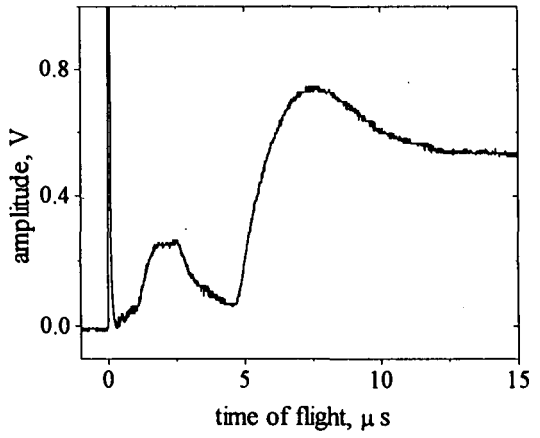

FIGURE 7. Ion collector signal of Ta plasma obtained by means of the charge collector of the type shown in figure 4a. Experimental conditions—see figure 4, $L_{coll} = 145$ cm.

ϵ is replaced by the product of grid transparencies, $\epsilon = \prod_{i=0}^{n} \epsilon_i$, where n is the number of grids, and taking $\bar{\gamma}/\bar{z} = 0$.

5.2. *Cylindrical Langmuir probes*

Langmuir probes are employed widely in the research of plasma in stationary systems (Ionov 1964; Chung *et al.* 1975). The moving cylindrical probe, from the point of using it in space investigation (on rockets and satellites), was analyzed by Hoegy and Wharton (1973). The possibility of using such probes in the studies of laser-produced plasma was presented in Koopman (1971) and Segall and Koopman (1973). Various types of Langmuir probes were constructed, the shapes and sizes of which depended on the plasma parameters and the quantity to be determined. The cylindrical Langmuir probe is a metallic thin-wire electrode, and it has no screening electrodes. The supply system is similar to the one for charge collector shown in figure 6a.

5.2.1. *Principle of operation*

The total current reaching the probe located in a streaming plasma is the sum of the ion component, I_i, and the electron component, I_e:

$$I_i = evS(1 + \bar{\gamma}/\bar{z})\bar{z}n_i \qquad \text{for } V < 0, \tag{37}$$

$$I_e = I_{e0}\exp[e(V - V_p)/kT_e] \qquad \text{for } V - V_p \leq 0, \tag{38}$$

where

$$I_{e0} = (\pi e S n_{e0}/4)\sqrt{8kT_e/\pi m_e}, \tag{39}$$

$S = 2rl$ is the cross-sectional area of the probe, r and l are the radius and the length of the probe, respectively, $n_{e0} = \Sigma z_j n_{i,j}$ is the electron density, V is the probe voltage, V_p is the plasma potential, and kT_e is the electron temperature of the plasma. The current-voltage characteristic is shown schematically in figure 8. For sufficient negative voltage of the probe, the electron component $I_e = 0$. This corresponds with the left side of the probe characteristic that operates in the saturation ion-current regime as a flat charge collector

https://doi.org/10.1017/S0263034600010053 Published online by Cambridge University Press

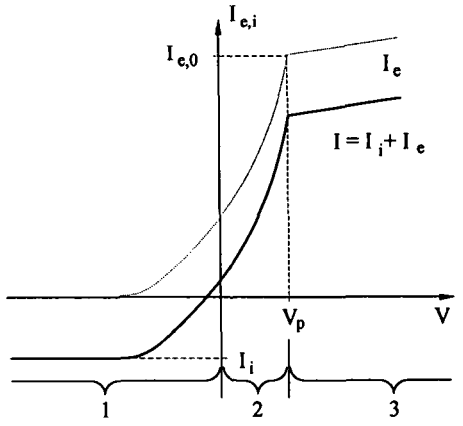

FIGURE 8. Schematic drawing of current-voltage characteristic of a Langmuir probe. 1 – ion attracted region ($V < 0$), 2 – repelled electron region ($V - V_p \leq 0$), 3 – attracted electron region ($V - V_p > 0$), V – probe voltage, V_p – plasma potential, I_e and I_i – electron and ion current, respectively.

[see equation (32)]. The electron temperature, T_e, can be evaluated from the semi-logarithmic plot of the repelled electron current of the current voltage characteristic:

$$kT_e = e(V - V_p)/\ln(I_e/I_{e0}). \tag{40}$$

It is valid with the assumption that $c_e \gg v > c_i$, where c_e and c_i are the electron and ion thermal velocities, respectively. The electron density, n_{e0}, can be calculated from equation (39). The time history of the plasma, $T_e = T_e(t)$ and $n_{e0} = n_{e0}(t)$, can be obtained calculating T_e and n_{e0} for several values of the time of flight t. In the case of the known $\bar{\gamma}/\bar{z}$ ratio, the ion density, n_i, also can be determined.

6. Visualization of ion emission areas

Investigations of interaction of high-intensity laser radiation ($I\lambda^2 > 10^{14}$ Wcm$^{-2}\mu$m^2) with high-Z targets have shown that the absorbed laser energy is used not only for the creation of hot plasma in the area of diameter close to the laser focus diameter, but it also is very effectively transported to the target material outside the laser focus. Experimental data have shown that, for Al targets irradiated with iodine laser radiation of intensities $I\lambda^2 \sim 10^{14}$–10^{15} Wcm$^{-2}\mu$m^2, the dimension of the area emitting ions was about ten times larger than the laser focus diameter (Mróz *et al.* 1994b). Such large dimensions of ion emitting areas proved high efficiency of the lateral energy transport. At least two sources of the lateral energy transport ought to be mentioned. The first is the energy transport by hot electrons, especially for intensities $I\lambda^2 > 10^{15}$ Wcm$^{-2}\mu$m^2. The hot electrons deposit their energy mainly on the surface around the focal spot. The bremsstrahlung and K_α radiation can deposit radiation energy around the laser focus and in the deeper parts of the target.

For visualization of the areas of ion emission, ion pinhole cameras in various configurations were prepared. The simplest camera was a pinhole camera with a pinhole diameter of about 15 μm located 60 mm from the track detector. This camera, located 15 mm from the target, gives 4× magnification, which is enough to observe ion emission areas, especially those enlarged by lateral heat transport. As a detector, the CR-39 polymer was used, for which the minimum energy of registered heavier ions is tens of keV/amu. For visualization of the birth place of ions with energies higher than the registration threshold of the

https://doi.org/10.1017/S0263034600010053 Published online by Cambridge University Press

track detector, a pinhole camera with an appropriate filter can be used. The use of energy filters decreases the ion flux, because of ion scattering. Additional ions crossing the foil change their charge state because they are "stripped" from electrons by the foil.

6.1. *Stroboscopic mass spectrography*

In the recent years, we have started a new method for visualizing the areas of ion emission, that is, the stroboscopic mass spectrography of the laser plasma. The apparatus built for this purpose can be used for visualization of the region of ion emission and neutral particle emission within a closely prescribed energy or velocity interval. The principal element of the apparatus is a generator of high-voltage pulses (from $U = 0$ up to 5 kV in amplitude) with the rise time $\delta t \cong 100$ ns and variable duration Δt within the range from 2 to 10 μs. This generator feeds pulsely an image converter cooperating with a pinhole camera with a hole diameter variable in the range of 50 to 100 μm (figure 9). The image converter is similar to the one in the TP, and it is composed of an amplifier based on the MCP and a luminescence screen deposited on fiber optics. A voltage pulse of an appropriate length, $\Delta t = t_2 - t_1$, applied at the time t_1, switches the converter in and out in the time t_2. Knowing the distance L from the source of plasma to the recording system, we can determine the velocity range of recorded ions as follows: $v_1 = L/t_1$, $v_2 = L/t_2$.

In the case of visualization of neutral particles, the charged particle, that is, electrons and ions, components first must be removed. This can be done by applying an electric or magnetic deflecting field. In this case, the TP may be used as a stroboscopic camera. The ion and electron components of the plasma will be removed in the deflecting chamber, in the region of parallel electric and magnetic fields.

At present, the method for stroboscopic mass spectrometry cannot give direct information about the quantity of ions because of the unknown secondary ion-electron emission coefficients. Additionally, ions of the same element but with different charge states give different contributions to the total luminescence of the image converter.

More information can be obtained by comparing the results from this method with the results from ion flux measurements by the track detector, which can give the number of ions, and with measurements of ion analyzers, from which ion energy distributions and percent composition can be estimated.

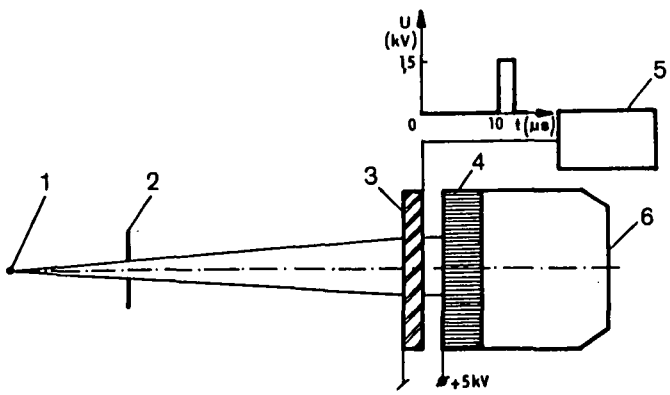

FIGURE 9. Stroboscopic ion pinhole camera. 1 – plasma, 2 – pinhole, 3 – microchannel plate, 4 – luminescence screen deposited on the fiber optics, 5 – high-voltage pulse generator, 6 – lensless photographic camera.

https://doi.org/10.1017/S0263034600010053 Published online by Cambridge University Press

7. Measurements of neutral atom fluxes

In the process of laser interaction with solid-state targets, a large quantity of neutral atoms expands from the heated area beside the plasma composed of ions and electrons. Rough estimations from the measurements made with the use of a Langmuir probe have shown that, for laser intensities $I\lambda^2 \sim 10^{14}$–10^{15} $\mathrm{Wcm^{-2}\mu m^2}$, about 80–90% of the material in the form of neutral atoms can expand from the target (Chvojka *et al.* 1994; Mróz *et al.* 1994). For high-Z targets, a large part of the neutral atoms expands from solid-state-density X-ray-created nonideal plasma (Ichimaru 1982). Measurements of the energy distribution and the quantity of neutral atoms as well as their total energy give additional information about the ionization and recombination processes in the solid-state-density plasma and about the absorbed laser-energy transport and redistribution during the target heating.

7.1. *Detector for neutral atoms*

A cylindrical detector for nonionized atoms (NAD) that allows the separation of charged and neutral particles from the expanding plasma is shown in figure 10 (Sarraf & Woodall 1978). The main element of the NAD is a deflecting chamber made as a copper cylindrical Faraday cup, cut longitudinally into two identical parts placed at a distance of about 3 mm. Both parts of the chamber are symmetrically polarized with the resistance $R = 4.3$ MΩ, limiting the current, with the voltage $\pm V$, which can be changed in the range of 0–5 keV, which is sufficient for the total separation of ions from electrons in the case when an input slit of diameter ∅4 mm and output slit of ∅5 mm are used. A weak longitudinal magnetic field, produced by two ring magnets, is applied to suppress the secondary electron emissions from the cylindrical surfaces of Faraday cups. The ion current from the ion collec-

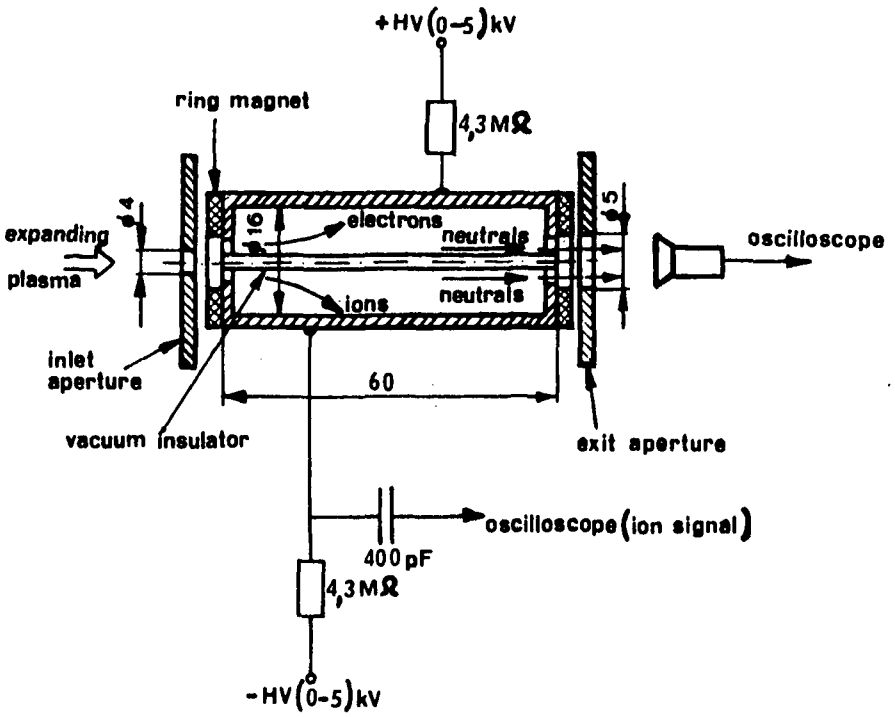

FIGURE 10. Cylindrical detector of nonionized atoms.

https://doi.org/10.1017/S0263034600010053 Published online by Cambridge University Press

tor (the negatively polarized part of the deflecting chamber) is passed through the separating condenser to the oscilloscope. The neutral component of the plasma (photons and neutral atoms) does not undergo deviation, and after passing through the output slit it falls on the detector. The role of the detector can be played by windowless electron multipliers, plasma calorimeters, or even fast BPYP-30 photodiodes with shallow connections and reverse polarization (Denus *et al.* 1986).

On the path of flight from the plasma to the detector, a separation of photons from atoms occurs, and, as a result, it is possible to register the velocity spectrum of the expanding atoms. While measuring the velocity spectrum of neutral atoms and energy carried by them, one should be sure that the plasma was totally split, because electron multipliers or calorimeters cannot differentiate between ions and neutral atoms. Two sources of information about the plasma splitting in the deflecting chamber exist (Denus *et al.* 1986), one of them being the ion pulse from the negatively polarized part of the deflecting chamber. Figure 11a shows a typical oscillogram from the flat ion collector with a negatively polarized grid ($I\lambda^2 \sim 5 \times 10^{13}$ Wcm$^{-2}\mu$m^2). The maximum of the ion current is due to the ions of veloc-

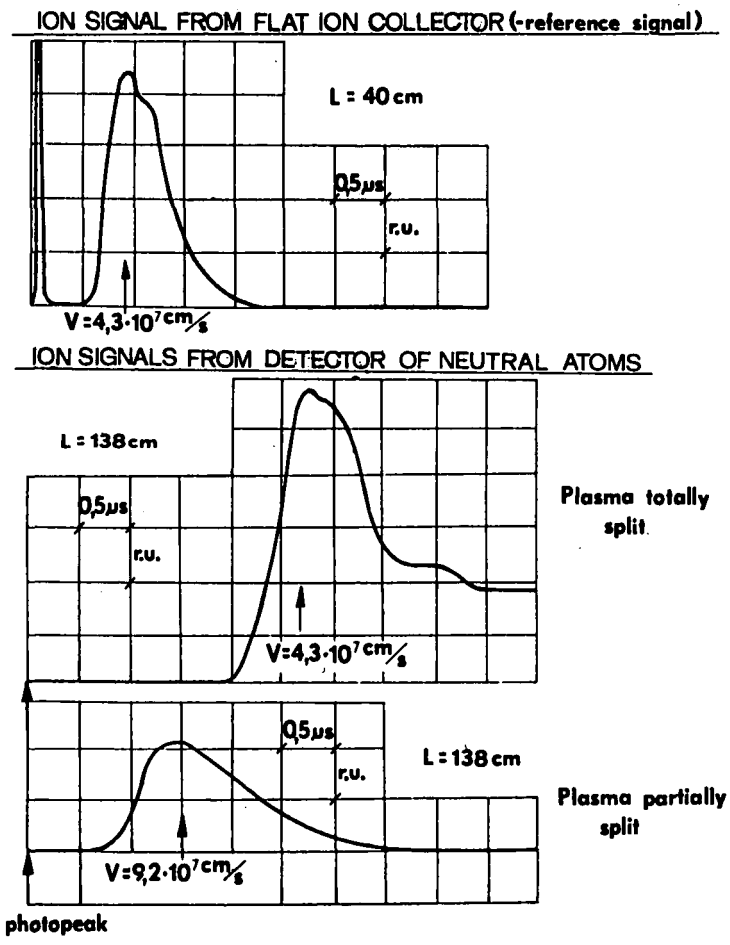

FIGURE 11. An ion signal from the NAD as a source of information about plasma splitting. (a) Ion collector signal from external collector; (b) ion signal from the NAD for the case of total splitting of the plasma; (c) ion signal from the NAD for the case of partial splitting of the plasma.

https://doi.org/10.1017/S0263034600010053 Published online by Cambridge University Press

ities $v \sim 4.3 \times 10^7$ cm/s. Figure 11b shows the ion signal from the NAD for the same shot, for the case of totally splitting the plasma. The maximum of the ion current, like in figure 11a, originates from the ions with velocities $v \sim 4.3 \times 10^7$ cm/s. In the case of partially splitting the plasma (figure 11c), the maximum of ion current from the NAD is shifted toward the higher velocities (in figure 11c, $v \sim 9.2 \times 10^7$ cm/s). The plasma with slower ions is too dense for a given splitting voltage and a given diameter of the input slit, and cannot be split fully. Figure 12a shows currents from the NAD. It consists of the photopeak, the ion component in the case when the plasma was not fully split (the peak corresponds to the velocity $v \cong 4.3 \times 10^7$ cm/s), and the component from neutral atoms from the plasma. In the case of total splitting of the plasma (figure 12b), the signal from the NAD consists of only the photopeak and the neutral atoms.

Sometimes, in the case of a low vacuum, a middle part of the signal from the NAD can appear as a result of a charge exchange and recombination processes in the deflecting chamber, even though the plasma was split totally.

8. Ion-induced secondary electron emission

The phenomenon of the secondary electron emission is one of the fundamental phenomena in particle–solid-state interactions. Secondary electrons may be induced from the surfaces of solids by impinging electrons, ions, and neutrals. The electron yield is characterized by the secondary electron emission coefficient, that is, the mean number of ejected electrons per incident particle. In the case of the ion-induced secondary emission, it is characterized by the secondary ion-electron emission coefficient, γ_z (also called the ion-induced secondary electron emission coefficient, or the secondary electron emission coefficient for short). This phenomenon is used in the detection of very small ion currents (in windowless electron multipliers, channel electron multipliers, and microchannel plates). However,

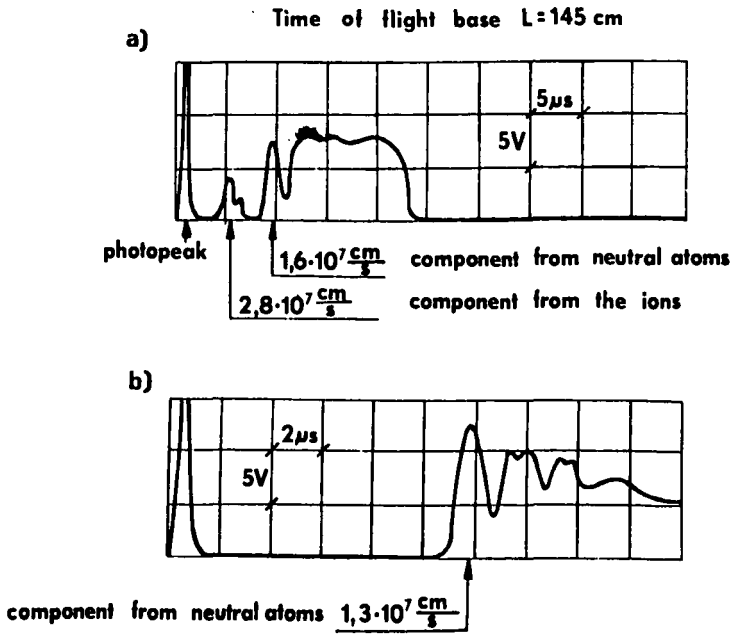

FIGURE 12. The currents from a detector of nonionized atoms; (a) for partially split plasma, (b) for fully split plasma.

https://doi.org/10.1017/S0263034600010053 Published online by Cambridge University Press

to obtain the magnitude of detected ion current, it is necessary to know the γ_z. The γ_z is the subject of many experimental investigations and theoretical treatments. But generally, no theory (the potential electron ejection mechanism is valid for the low kinetic energy of ions, below about 500 eV, and the kinetic electron ejection mechanism is valid for the higher kinetic energy of ions, above 500 eV) can explain some experimentally observed behavior of γ_z over a wide energy range (from tens of eV to a few MeV) of incident ions. Besides, for a given ion–metal combination, the γ_z consists of the almost constant contribution of the potential electron emission coefficient, γ_p, and the kinetic electron emission coefficient, γ_k, when the ion kinetic energy exceeds a certain threshold value, that is, $\gamma_z = \gamma_p + \gamma_k$. Most published information refers to the atomically clean pure metallic surfaces impacted mainly by ions of gases (noble gases, hydrogen, nitrogen, and oxygen).

A comprehensive collection of experimental results on the potential electron ejection was prepared by McDaniel (1964). It was based mainly on Hagstrum's (1953a,b, 1954) experimental results and theoretical treatments, and Parker's (1954) experimental investigations. The analysis and experimental investigation of the potential electron ejection mechanism also can be found in Arifov *et al.* (1973). The basic conclusions from the above works are as follows: The state of the surface of metal has evident influence on γ_z; γ_z weakly depends on the kinetic energy range of incident ions, and it increases with increasing ionization energy of the incident ions; for multicharged ions, the γ_z is proportional to the charge state to the second power, and the γ_z linearly depends on the total neutralization energy of multicharged ions; γ_z due to mixed ions (multicharged noble gas ions with the addition of low-Z element ions) is much lower than the γ_z for pure multicharged ions.

Also, in the case of the kinetic electron ejection mechanism, that is, for the kinetic energy of incident ions above 500 eV, the experiments were concerned mainly with noble gas, atomic H, N, O, C, and Hg; diatomic H_2, N_2, and O_2; and polyatomic ions (Higatsberger *et al.* 1954; Magnuson & Carlston 1963; Schram *et al.* 1966; Begrambekov *et al.* 1969; van Gorkom & Glick 1970), in the kinetic energy range only below 90 keV, from various metals (Ni, Cu, Al, W, Ag, Sn, Mg, Cd, Au, Mo, and Nb) and alloys (Cu-Be, Ag-Mg, and Nichrom V). Hasselkamp *et al.* (1980) investigated the γ_z from Al, Cu, Ag, W, and Au induced by H^+, H_2^+, H_3^+, He^+, Ne^+, and Ar^+ ions in the energy range from 80 keV to 1 MeV. Thornton and Anno (1977) measured the γ_z from Al, V, Fe, Mo, Nb, and 316 stainless steel induced by $^1H^+$ and $^2H^+$ ions in the ion kinetic energy range from 0.5 to 2.5 MeV.

However, in high-Z laser-produced plasma, ions with charge states of 50 or more and with kinetic energy reaching some MeV were produced and recorded (Woryna 1995; Laska *et al.* 1995; Haseroth *et al.* 1995). In our experiments, the windowless electron multiplier (WEM) EMI 9643/2B and THORN EMI 226M-type one with CuBe dynodes were used as detectors. Considering those detectors, to obtain quantitative information about plasma parameters, it was necessary to know the γ_z in a wide range of charge states and kinetic energy of ions incident on the CuBe cathode of the WEM. Thus, our review will comprise only the experimental investigations of secondary ion-electron emission from CuBe. A short review of the experimental results of such types was previously published by Baumgartner and Hubert (1976).

Higatsberger *et al.* (1954) investigated the secondary emission from AgMg and CuBe alloys (used in the WEMs because of high γ_z) induced by He^+, $^{20}Ne^+$, $^{22}Ne^+$, Ar^+, Ar^{2+}, Kr^+, Xe^+, Hg^+, Hg^{2+}, O^+, O_2^+, and H_2^+ over the kinetic energy range from about 1 to 8 keV. The γ_z kinetic energy dependences smoothly increase with energy. In addition, the authors found the isotope effect for $^{20}Ne^+$ and $^{22}Ne^+$, with the γ_z for $^{20}Ne^+$ slightly higher than that for $^{22}Ne^+$ ions.

Schram *et al.* (1966) investigated the efficiencies of the WEM with Venetian blinds and the CuBe dynodes comparing the WEM signals with those of a Faraday cup caused by multi-

https://doi.org/10.1017/S0263034600010053 Published online by Cambridge University Press

charged noble gas ions (He^+ and He^{2+}, Ne^+ to Ne^{3+}, Ar^+ to Ar^{5+}, Kr^+ to Kr^{7+}, and Xe^+ to Xe^{9+}). The kinetic energy of the ions was in the range of 3 to 90 keV. They found that γ_z is independent of the charge state of ions, and that the γ_z ion velocity dependence is linear. All straight lines for the different gases cross the velocity axis at the same value $v_0 = 5.5 \times 10^6$ cm/s, which is the threshold velocity for the kinetic electron ejection. The slopes of the lines are proportional to $M^{1/2}$ (where M is the mass of an incident ion); thus the $\gamma_z \propto M^{1/2}$.

Van Gorkom and Glick (1970) performed similar investigations as Schram *et al.* (1966). The γ_z was determined for atomic (He^+, Ne^+, Ar^+ and Ar^{2+}, Kr^+, Xe^+, H^+, C^+, N^+, and O^+), diatomic (H_2^+, N_2^+, and O_2^+), and polyatomic ions incident on CuBe with the kinetic energy range of 2 to 10 keV. They found that γ_z for Ar^+ and Ar^{2+} lie on the same straight line, as in the Schram *et al.* (1966) experiment. They concluded that the initial charge state of an ion seems to be unimportant for γ_z, as was predicted by Parilis and Kishinevskii (1960). The threshold velocity was estimated to be $v_0 = 4 \times 10^6$ cm/s. The behavior of the atomic ions was different from that of diatomic and polyatomic ions. Diatomic and polyatomic ions are more efficient to eject secondary electrons than atomic ions.

Lao *et al.* (1972) measured the gain of the WEM with CuBe dynodes for 24 atomic ions of all groups of the periodic system at a given kinetic energy, 5.1 keV, relative to Ar^+ ions. The gain decreases with increasing mass for elements within the periodic groups. The general trend of the γ_z for different groups was as follows: IIIA(B) < IVA(C, Si, Ge, Sn, Pb) < VIIA(Cl, Br, I) < VA(N, P, As, Sb) < VIA(O, S, Se) < VIIIA(He, Ne, Ar, Kr, Xe). The total spread in the gain of about three was reported.

Fehn (1976) investigated the variance of γ_z with an atomic number of ions incident on three materials used most often as dynode materials: CuBe, Al, and Ni. The investigations were performed for ions from Li to Pb (22 elements) with the kinetic energy of 8.0 keV. For all three dynode materials an increase of γ_z toward the higher-Z elements was found. However, CuBe shows the strongest increase, followed by Al and Ni. This increase is not smooth, but it shows a periodic increase. The locations of maxima and minima appear to be independent of the dynode material. A combined set of experimental data from Lao *et al.* (1972) and obtained by Fehn (1976), after extrapolation to γ_z for a constant velocity and considering an adjustment factor, are very consistent. The comparison of the periodicity with the periodic groups of elements shows that the maxima appear for noble gases and for the IVB group, and the minima for the IIA and IIB groups. The comparison of the results obtained for γ_z showed good agreement with the periodicity found theoretically for electronic stopping by Baklitskii and Parilis (1972).

Cano (1973) investigated the ion-induced secondary electron emission from gas-covered Au, Mo, and CuBe surfaces by H^+, C^+ to C^{6+}, Al^+ to Al^{10+}, Cu^+ to Cu^{9+}, and Ta^+ to Ta^{3+} from laser-produced plasma in the energy range from 0.3 to 22.4 keV. The results of the measurements are in poor agreement or partially even in disagreement with the theory and the interpretation of other authors. The main conclusions made by the author can be summarized as follows: The γ_z kinetic energy of ion dependence is nonlinear for ions with charge states from 1 to 5 incident onto CuBe with energy below 5 keV; for ions with charge states $z > 5$ incident onto CuBe, $z > 2$ onto Mo, and in all cases for Au, the relations γ_z ion energy are linear, and γ_z are nearly independent of kinetic energy of incident ions; in general, with an increased charge state of ions the slope of γ_z dependences decreases and may change its sign; an empirical fit for the charge state $z = 5$ (for Mo and CuBe) shows that $\gamma_z \propto M^{-x}$, where $2/5 \leq x \leq 1/2$; the potential electron ejection mechanism is dominant over the kinetic electron ejection mechanism in the range of ion energy used in the experiment. The experimental results obtained for low charge state $z < 3$ and high mass

https://doi.org/10.1017/S0263034600010053 Published online by Cambridge University Press

$A \geq 27$ are only in qualitative agreement with the Parilis and Kishinevskii theory of secondary electron emission. For higher charge states, $z \geq 4$, or low mass, $A \leq 12$, there is no agreement. Nevertheless, many experimentors used those results for processing experimental data.

Dietz and Sheffield (1975) investigated the ion-induced secondary electron emission from Al_2O_3 and BeO by Li^+, Na^+, K^+, Rb^+, Cs^+, and Ni^+ isotopes as a function of ion velocity. The obtained data are consistent with the Parilis and Kishinevskii theory of a common threshold velocity, which was estimated to be $v_0 = 5.5 \times 10^6$ cm/s. The results demonstrate the absence of the isotope effect on the γ_z. The authors used data from Schram *et al.* (1966) for noble gases to compute the threshold velocity. The fit gives $v_0 = 5.1 \times 10^6$ cm/s, which is in excellent agreement with their v_0 for BeO. They also investigated the influence of the incident angle on γ_z, and they found that singly charged ions with an energy of 30 keV incident on the BeO surface at 70° produce three times as many secondary electrons as they do at 0°. The results for each kind of ion differ significantly from each other, and they also differ somewhat from the sec Θ relationship. At the grazing angle, the yields are very high.

Knapp (1995) presented the results of a systematic study of secondary ion-electron emission yields from Ar^{z+}, Xe^{z+}, and Th^{z+} ions normally incident on a clean gold surface (Aumayr *et al.* 1993; Kurz *et al.* 1994). For ions with velocity $v > 2.5 \times 10^6$ cm/s, the data are well represented by an empirical formula derived from earlier studies (Kurz *et al.* 1992, 1993):

$$\gamma = c_1/\sqrt{v} + \gamma_\infty, \tag{41}$$

where c_1 is an empirical constant and γ_∞ is the velocity-independent emission. The data deviate significantly from the fit at very low velocities ($v > 2.5 \times 10^6$ cm/s), but at $v \approx 5 \times 10^7$ cm/s the γ/z ratio for $Xe^{z+} \rightarrow$ Au takes the following values: about 1.7, 1.9, and 3.0 for $z = 34$, 40, and 50, respectively, and they show decreasing tendency with an increase of ion velocity.

Equations (32)–(35), (37), and (38) contain the $\bar{\gamma}/\bar{z}$ ratio. The values were investigated in several experiments. On the basis of experimental results on laser-driven compression of spherical glass shells, Charatis (1975) stated that $\bar{\gamma}/\bar{z} \cong 1$. Goforth (1976) used the plane electrostatic analyzer to calibrate the charge collectors for mass and end energy recovery measurements. The author found that the $\bar{\gamma}/\bar{z} = 0.9$ for O^{7+} and O^{8+} ions at normal incidence and the $\bar{\gamma}/\bar{z}$ was independent of ion velocity in the range $(0.25\text{–}1.4) \times 10^8$ cm/s, to within 20% uncertainty, in agreement with results given by Cano (1973). Other multicharged ions also gave approximately the same value of $\bar{\gamma}/\bar{z}$, but the protons gave $\bar{\gamma}/\bar{z} \cong 3$ in that velocity range, and were in rough agreement with Barnett and Ray (1972) measured on the gas-covered Cu. Thus, for processing the ion collector results we used $\bar{\gamma}/\bar{z} = 1$.

From the experimental results presented above, it is seen that: For polycrystalline metals bombarded by ions with kinetic energies lower than 100 keV, only the Parilis and Kishinevskii theory is in satisfactory agreement with the experiments; the γ_z is critically dependent on the state of the surface of the metal; the γ_z varies approximately as sec Θ; the bulk properties of a metal surface influence the yield of secondary electrons (electronic band structure of the surface layer, chemical uniformity, thickness of an oxide layer, topographical smoothness, and crystalline structure of the surface) (Dietz & Sheffield 1975).

We can conclude that the measurements of the γ_z for a wide range of incident multicharged ion–CuBe combinations and a large energy scale of incident ions are indispensable. The lack of such dependences makes processing experimental data from the WEM

https://doi.org/10.1017/S0263034600010053 Published online by Cambridge University Press

impossible considering the need to obtain quantitative information about plasma parameters.

9. Summary

The equipment presented in this paper, intended for corpuscular diagnostics of laser-produced plasma, was developed and constructed at the IPPLM. It has proved to be very useful for investigating the ion component and neutral atom fluxes emitted from laser-produced plasma. It has been applied in a series of laboratories and experiments, for example, at IPPLM in the experiments on laser-driven compression of spherical targets and investigations of Nd and CO_2–laser interaction with materials with various atomic numbers; at the Lebedev Physics Institute (FIAN) in the experiments on laser-driven compression of spherical targets in the KALMAR and DELFIN laser systems; at the Institute of Physics of the Academy of Science of the Czech Republic in the experiments on the PERUN–iodine laser system (first, second, and third harmonics) interaction with materials of high atomic numbers; and at the ITEP and TRINITY on CO_2 lasers.

The results of the experimental investigations, obtained by means of the measuring equipment described, will enable us to:

- measure the energy distributions of individual ion species and, on this basis, determine the plasma composition and ionization degree (IEA, TP);
- measure the angular distributions of plasma expansion (charge collectors, Langmuir probes);
- determine the plasma parameters in the laser focus spots (IEA, charge collectors);
- determine the plasma parameters at long distances from the target (Langmuir probes);
- image the ion-emitting volume (stroboscopic and common ion pinhole camera);
- acquire information on the ionization–recombination processes occurring in the plasma.

However, in order to get accurate quantitative data on the basis of the obtained experimental results, a knowledge of the secondary electron emission coefficient, γ_z, is required. Therefore, it is necessary to measure the dependences of γ_z on the atomic Z number of highly ionized atoms, in a wide range of ion energy, for the materials applied for dynodes of windowless electron multipliers (CuBe in the given case) as well as the material applied for collectors, both in the charge collectors and the Langmuir probes.

REFERENCES

Afanas'ev, V.P. & Yavor, S.Ya. 1978 *Elektrostatitcheskie Energoanalizatory dla Putchkov Zarazhennych Tchastits* (Nauka, Moscow) (in Russian).

Amdidouche, Y. *et al.* 1992 *Rev. Sci. Instrum.* **63**, 2838.

Arifov, U.A. *et al.* 1973 *Sov. J. Tech. Phys.* **53**, 375.

Aumayr, F. *et al.* 1993 *Phys. Rev. Lett.* **71**, 1943.

Baklitskii, B.E. & Parilis, E.S. 1972 *Radiat. Eff.* **12**, 137.

Baldis, H.A. *et al.* 1991 *Handbook of Plasma Physics, Vol. 3*, A. Rubenchik and S. Witkowski, eds. (North-Holland Publishers, Amsterdam–London–New York–Tokyo), p. 435.

Barabash, L.Z. *et al.* 1989 *Sov. J. Atom. Energy* **66**, 107.

Barnett, C.F. & Ray, J.A. 1972 *Nuclear Fusion* **12**, 65.

Baumgartner, W.E. & Hubert, W.K. 1976 *J. Phys. E: Sci. Instrum.* **9**, 321.

Begrambekov, L.B. *et al.* 1969 *Sov. Plasma Phys.* **2**, 42.

https://doi.org/10.1017/S0263034600010053 Published online by Cambridge University Press

BILLINGE, R. *et al.* 1990 Report CERN 90-01, Geneva.

BOCHER, J.L. 1978 *Optics Comm.* **24**, 297.

BRAAMS, C.M. 1964 *Nucl. Instrum. Methods* **26**, 83.

BUSQUET, M. 1982 *Phys. Rev. A* **25**, 2302.

BYKOVSKII, YU.A. & NEVOLIN, V.N. 1985 *Lazernaja Mass-spektrometria* (Energoatomizdat, Moscow) (in Russian).

CANO, G.L. 1973. *J. Appl. Phys.* **44**, 5293.

CHANG, C.T. *et al.* 1977 *Plasma Phys.* **19**, 1129.

CHARATIS, G. 1975 *Plasma Physics and Controlled Nuclear Fusion Research, Vol. 2* (IAEA, Vienna), p. 317.

CHOWDHURY, S.S. *et al.* 1980 *J. Phys. E: Instrum.* **13**, 1099.

CHUNG, P.M. *et al.* 1975 *Electric Probes in Stationary and Flowing Plasmas: Theory and Application* (Springer-Verlag, Berlin–Heidelberg–New York).

CHVOJKA, M. *et al.* 1994 *Czech. J. Phys.* **44**, 851.

DECOSTE, R. *et al.* 1986 *Phys. Fluids* **29**, 328.

DECOSTE, R. & RIPIN, B.H. 1977 *Rev. Sci. Instrum.* **48**, 232.

DENUS, S. *et al.* 1977 *J. Tech. Phys.* **18**, 25.

DENUS, S. *et al.* 1986 *Laser Part. Beam* **4**, 507.

DIETZ, L.A. & SHEFFIELD, J.C. 1975 *J. Appl. Phys.* **46**, 4361.

EHLER, W. *et al.* 1980 *J. Phys. D: Appl. Phys.* **13**, L29.

EIDMANN, K. *et al.* 1984 *Phys. Rev. A.* **30**(5), 2568.

EIDMANN, K. *et al.* 1900 *Phys. Fluids* **B2**(1), 208.

FARNY, J. 1979 IPPLM Report No. 11/79/11, Warsaw (in Polish).

FARNY, J. & WORYNA, E. 1987 IPPLM Report No. 3/87; 18th European Conference on Laser Interaction with Matter, 4–8 May, Prague, Czechoslovakia.

FEHN, U. 1976 *Int. J. Mass Spectrom. Ion Phys.* **21**, 1.

FLEISCHMANN, H.H. *et al.* 1965 *Nucl. Fusion* **5**, 349.

GOFORTH, R.R. 1976 *Rev. Sci. Instrum.* **47**, 548.

GOLDSACK, T.J. *et al.* 1982 *Optics Comm.* **42**, 55.

VAN GORKOM, M. & GLICK, R.E. 1970 *Int. J. Mass Spectrom. Ion Phys.* **4**, 203.

GREEN, T.S. 1970 *Plasma Phys.* **12**, 877.

GRUN, J. 1986 *Phys. Fluids* **29**, 3390.

GUPTA, P.D. *et al.* 1986 *Phys. Rev. A* **34**, 4103.

GUSINOV, M.A. *et al.* 1978 *Appl. Phys. Lett.* **39**, 800.

HAGSTRUM, H.D. 1953a *Phys. Rev.* **89**, 244.

HAGSTRUM, H.D. 1953b *Phys. Rev.* **91**, 543.

HAGSTRUM, H.D. 1954 *Phys. Rev.* **96**, 325.

HANKELMANN, T. *et al.* 1992 *Rev. Sci. Instrum.* **63**, 2828.

HASEROTH, H. *et al.* (in this issue).

HASEROTH, H. & HORA, H. 1993 *Advances of Accelerator Physics and Technologies*, H. Scopper, ed. (World Scientific, Singapore), p. 466.

HASEROTH, H. *et al.* 1995 *Laser Interaction with Matter, Proc. 23rd European Conference*, S.J. Rose, ed., St. John's College, Oxford, U.K., 19–23 September, Institute of Physics Conference Series Number 140, (Institute of Physics Publishing, Bristol and Philadelphia), p. 293.

HASSELKAMP, D. *et al.* 1981 *Nucl. Instrum. Meth.* **180**, 349.

HEROLD, H. *et al.* 1981 *Rev. Sci. Instrum.* **52**, 24.

HIGATSBERGER, M.J. *et al.* 1954 *J. Appl. Phys.* **25**, 883.

HOEGY, W.R. & WHARTON, L.E. 1973 *J. Appl. Phys.* **44**, 5365.

ICHIMARU, S. 1982 *Rev. Modern Phys.* **54**, 1017.

IONOV, I.I. 1964 *Sov. J. Tech. Phys.* **34**, 669.

https://doi.org/10.1017/S0263034600010053 Published online by Cambridge University Press

JOSHI, C. *et al.* 1979 *Appl. Phys. Lett.* **34**, 625.

KIEFFER, J.C. *et al.* 1985 *J. Appl. Phys.* **58**, 4736.

KNAPP, D.A. 1995 *Physics with Multiply Charged Ions*, D. Liesen, ed., NATO ASI Series, Series B: Physics Vol. 348 (Plenum Press, New York), p. 143.

KOOPMAN, D.W. 1971 *Phys. Fluids* **14**, 1707.

KOZLOV, I.G. 1971 *Metody Energeticheskogo Analiza Elektronnych Potokov* (Atomizdat, Moscow) (in Russian).

KOZLOV, O.V. 1969 *Elektricheskii Zond v Plazmie* (Atomizdat, Moscow) (in Russian).

KOZOCHKIN, S.M. *et al.* 1993 Kurchatov Institute Report IEA-5635/7 (Moscow).

KRUER, W.L. 1988 *The Physics of Laser Plasma Interaction*, Frontiers in Physics, Vol. 73 (Addison-Wesley, Reading, MA).

KURZ, H. *et al.* 1992 *Phys. Rev. Lett.* **69**, 1140.

KURZ, H. *et al.* 1993 *Phys. Rev. A* **48**, 2182.

KURZ, H. *et al.* 1994 *Phys. Rev. A* **49**, 4693.

KUTNER, V.B. *et al.* 1992 *Rev. Sci. Intrum.* **63**, 2835.

LAO, R.C. *et al.* 1972 *Int. J. Mass Spectrom. Ion Phys.* **10**, 309.

LÁSKA, L. *et al.* 1994 *Appl. Phys. Lett.* **65**, 691.

LÁSKA, L. *et al.* 1995 *6th International Conference on Ion Sources ICIS'95*, Contribution No. B08-S1, 10–16 September, Whistler, B.C.

LEWIS, C.L.S. *et al.* 1982 *J. Phys. D: Appl. Phys.* **15**, 69.

MAGNUSON, G.D. & CARLSTON, C.E. 1963 *Phys. Rev.* **129**, 2403.

MCDANIEL, E.W. 1964 *Collision Phenomena in Ionized Gases* (John Wiley & Sons, Inc., New York–London–Sydney).

MAKAROV, K.N. *et al.* 1994 *ZhETF* **106**, 1649 (in Russian).

MRÓZ, W. *et al.* 1989 *Laser Part. Beam* **7**, 3.

MRÓZ, W. *et al.* 1992a *Laser Part. Beam* **10**, 689.

MRÓZ, W. *et al.* 1992b *J. Tech. Phys.* **33**, 67.

MRÓZ, W. *et al.* 1994a *Rev. Sci. Instrum.* **65**, 1272.

MRÓZ, W. *et al.* 1994b *Laser Part. Beam* **12**, 421.

OLSEN, J.N. *et al.* 1973 *J. Appl. Phys.* **44**, 2275.

PARILIS, E.S. & KISHINEVSKII, L.M. 1960 *Sov. Phys.-Solid State* **3**, 1219.

PARKER, J.H. 1954 *Phys. Rev.* **93**, 1148.

PARYS, P. *et al.* 1995a *Laser Interaction with Matter, Proc. 23rd European Conference*, S.J. Rose, ed., St. John's College, Oxford, U.K., 19–23 September, Institute of Physics Conference Series Number 140 (Institute of Physics Publishing, Bristol and Philadelphia), p. 371.

PARYS, P. *et al.* 1995b *Laser Interaction with Matter, Proc. 23rd European Conference*, S.J. Rose, ed., St. John's College, Oxford, U.K., 19–23 September, Institute of Physics Conference Series Number 140 (Institute of Physics Publishing, Bristol and Philadelphia), p. 375.

PEARLMAN, J.S. 1977 *Rev. Sci. Instrum.* **48**, 1064.

PELAH, I. 1976 *Phys. Lett.* **59A**, 348.

RAVEN, A. *et al.* 1980 *Rev. Sci. Instrum.* **51**(3), 351.

RIPIN, B.H. *et al.* 1980 *Phys. Fluids* **23**, 1012.

SADOWSKI, M. *et al.* 1976 *J. Tech. Phys.* **17**(3), 315.

SARRAF, S. & WOODALL, D.M. 1978 *Rev. Sci. Instrum.* **49**, 1147.

SCHRAM, B.L. *et al.* 1966 *Proc. 7th Int. Conf. on Phenomena in Ionized Gases*, Vol. 1 (Beograd), p. 170.

SEGALL, S.B. & KOOPMAN, D.W. 1973 *Phys. Fluids* **16**, 1149.

SHARKOV, B.YU. *et al.* 1992 *Rev. Sci. Instrum.* **28**, 2841.

SHEARER, J.W. & BARNES, W.S. 1972. *Laser Interact.* **I**, 307.

SIGEL, R. *et al.* 1990 *Phys. Fluids* **B2**(1), 199.

SLATER, D.C. 1978 *Rev. Sci. Instrum.* **49**, 1493.

https://doi.org/10.1017/S0263034600010053 Published online by Cambridge University Press

TALLENTS, G.J. 1978 *J. Phys. E: Sci. Instrum.* **11**, 769.

THOMSON, J.J. 1911 *Philos. Mag.* **21**, 225.

THORNTON, T.A. & ANNO, J.N. 1977 *J. Appl. Phys.* **48**, 1718.

WEBER, R. *et al.* 1986 *Rev. Sci. Instrum.* **57**, 1251.

WICKENS, L.M. & ALLEN, J.E. 1981 *Phys. Fluids* **24**, 1894.

WOŁOWSKI, J. *et al.* 1985 *Trudy FIAN* **149**, 125 (in Russian).

WORYNA, E. *et al.* 1995 *Laser Interaction with Matter, Proc. 23rd European Conference*, S.J. Rose, ed., St. John's College, Oxford, U.K., 19–23 September, Institute of Physics Conference Series Number 140 (Institute of Physics Publishing, Bristol and Philadelphia), p. 463.

https://doi.org/10.1017/S0263034600010053 Published online by Cambridge University Press